

5-15-54  
NACA RM E54A29

6871

201  
Copy  
RM E54A29

0143306

TECH LIBRARY KAFB, NM

  
**NACA**

# RESEARCH MEMORANDUM

PHOTOGRAPHIC STUDY OF ROTARY SCREAMING AND OTHER  
OSCILLATIONS IN A ROCKET ENGINE

By Theodore Male, William R. Kerslake, and Adelbert O. Tischler

Lewis Flight Propulsion Laboratory  
Cleveland, Ohio

Classification cancelled (or changed to *UNCLASSIFIED*)

By Authority of *NASA Tech Pub Announcement #135*  
(OFFICER AUTHORIZED TO CHANGE)


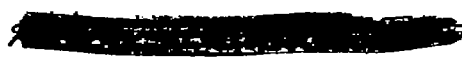
By *W. R. Kerslake*  
NAME AND

*W. R. Kerslake*  
GRADE OF OFFICER MAKING CHANGE

*27 May 61*  
DATE

  
**NATIONAL ADVISORY COMMITTEE  
FOR AERONAUTICS**

WASHINGTON

May 25, 1954  
  




0143306

NACA RM E54A29

~~CONFIDENTIAL~~

## NATIONAL ADVISORY COMMITTEE FOR AERONAUTICS

RESEARCH MEMORANDUM

## PHOTOGRAPHIC STUDY OF ROTARY SCREAMING AND OTHER OSCILLATIONS

## IN A ROCKET ENGINE

By Theodore Male, William R. Kerslake, and Adelbert O. Tischler

## SUMMARY

An investigation of combustion oscillations was conducted using white fuming nitric acid and a hydrocarbon fuel in a 1000-pound-thrust rocket engine. Photographs were taken of the screaming combustion through a transparent section of the chamber with a 40,000-frame-per-second motion-picture camera and a moving-film camera. Supporting information was obtained by pressure measurements and ion gap measurements.

A rotary or tangential mode of oscillation in the frequency range of 4000 to 6000 cycles per second was revealed by the 40,000-frame-per-second photographs. In addition to rotary oscillations, longitudinal oscillations of approximately 1000 cycles per second and another lateral mode of approximately 10,000 cycles per second were revealed by the streak photographs from the moving-film camera.

Erosion of the plastic chamber walls indicated heat-transfer rates during screaming operation several times as great as during normal operation. Furthermore, screaming in which the rotary mode was dominant caused greater erosion per unit time than screaming in which the longitudinal mode was dominant.

## INTRODUCTION

The occurrence of high-frequency combustion-driven oscillations in rocket combustion chambers has become a major problem in the development of large thrust units. These oscillations are commonly known as screaming because they are usually accompanied by a characteristic intense squeal or high-frequency sound which is audible above the engine exhaust roar. Screaming, when it occurs, generally increases specific impulse and causes greatly increased rates of heat transfer to the walls of the rocket combustion chamber which usually result in destruction of the chamber.

~~CONFIDENTIAL~~

54-2365

3168

T-1  
C-1

There is presently no positive cure for the screaming difficulty. In part, this is due to the fact that the combustion mechanisms which drive the high-frequency oscillations are not well defined. A number of papers have recently been published (refs. 1, 2, and 3) which yield considerable information about the high-frequency combustion oscillation phenomena. Ellis and others (ref. 1) showed simultaneous pressure measurements at a series of points in a screaming rocket combustion chamber which clearly indicate the sustained propagation of a pressure wave through the rocket combustion chamber with reflections of the pressure wave at the injector and nozzle ends of the chamber. Reference 2 gives a correlation of longitudinal oscillation frequency with the length of the combustion chamber. The observation of the longitudinal mode in these combustion chambers, however, does not preclude the existence of the many other possible modes of oscillation.

Berman and Cheney (ref. 3) photographed oscillations in a rocket engine through a quartz window in the chamber by means of the slit and moving-film technique. These records show that small pressure disturbances in the chamber can develop into pressure and flow oscillations of considerable amplitude. Their estimation of the pressure ratios based on measurements of the propellant flow velocity before and after the passage of the wave (a shock) indicates that the pressure ratios across the wave disturbance are of the order of  $1\frac{1}{2}$ .

Combustion-driven oscillations have also become a problem in the use of afterburners for turbojet engines (refs. 4 to 6). Reference 6 showed a correlation between the oscillation frequencies observed in several afterburner configurations and the tangential acoustical modes of oscillation in a cylindrical chamber. In the afterburner configurations the oscillations were suppressed by use of a perforated shell acoustical baffle at the burner walls.

In order to gain further information on the combustion reactions in a rocket engine under screaming conditions, direct motion pictures of the combustion in a 1000-pound-thrust acid-hydrocarbon rocket engine equipped with a plastic chamber section have been obtained with a 40,000-frame-per-second camera. In addition, streak photographs of the combustion were made with a moving-film camera. This report presents these photographs along with an analysis and discussion of the results.

## APPARATUS

### Rocket Engine and Instrumentation

The rocket engine used for the experimental investigation of screaming combustion was a 1000-pound-thrust uncooled rocket using white fuming nitric acid and JP-3 fuel as propellants. Hypergolic ignition was

accomplished by filling the fuel line ahead of the propellant control valve with furfuryl alcohol on which combustion persisted for about 0.7 second before entrance of JP-3 fuel.

The rocket engine assembly was held together by tie rods and flanges as shown in figure 1. Rubber gaskets were used to seal the transparent plastic section to adjacent components of the combustion chamber. The  $5\frac{1}{2}$ -inch-long transparent section was made of polymethylmethacrylate, a clear plastic. It was mounted flush to the injector face, except for the few runs when it was mounted near the nozzle. The lens effect, apparent in the photograph, was considered in the analysis of the combustion photographs and was nullified by proper selection of reference positions.

The length of the combustion chamber from the injector to the throat of the nozzle was 23 inches, and the internal diameter was 4 inches. The characteristic length  $L^*$  of the chamber was 116 inches for a throat diameter of 1.76 inches.

The injector shown in figure 2 consisted of 24 sets of radial triplet impinging jets. Each set had two oxidant jets impinging on one fuel jet, with  $45^\circ$  between each oxidant jet and the axially directed fuel jet. The propellants were pumped by high-pressure helium gas, and the pressure differential across the injector orifices was approximately 100 pounds per square inch for both oxidant and fuel.

Rocket engine thrust (accuracy of  $\pm 2$  percent) was measured by a strain gage load cell. Propellant flows (accuracy,  $\pm 5$  percent) were measured with orifices equipped with strain gage differential pressure transducers, and chamber static pressure was measured by a strain gage transducer (accuracy,  $\pm 5$  percent).

#### Special Instrumentation

Most of the combustion oscillation data were obtained by photographic methods; additional information was obtained by pressure and ion gap measurements.

40,000-frame-per-second camera. - The direct light from the combustion was photographed through the transparent section of the chamber by the NACA high-speed motion-picture camera (ref. 7) at 40,000 frames per second. This camera was used to magnify the time scale of a selected short sequence (about 1/100 sec) of the rocket combustion in order to identify and analyze the high-frequency oscillations.

Two views of the chamber were recorded simultaneously in order to accomplish a three-dimensional analysis of the combustion phenomena.

3168

CV-1 back

Figure 3 illustrates how this was accomplished by viewing the chamber from positions approximately  $90^\circ$  apart and then merging the two optical light paths by suitably placed mirrors to position the images side by side on the film. Because of the geometry of this particular configuration, the angle between the two views was actually about  $84^\circ$ .

The NACA high-speed camera is a rotating drum type of camera with optical compensation and employs standard 8-millimeter film. The optical compensation, described in reference 7, utilizes a focal-plane shutter that does not expose all parts of the photograph simultaneously. However, the motion of the focal-plane shutter was set up to be in the direction of propellant flow; consequently, for each station along the length of the transparent section, both top and side views were recorded simultaneously.

Moving-film streak photography. - Oscillation frequencies, shock velocities, and propellant flow velocities were measured from strip film records of the rocket combustion by moving a 16-millimeter film past the image of a slit at speeds of 20 to 35 feet per second. The slit was a 1/4 inch wide window mounted axially full length along the center of the transparent section of the chamber. As diagrammed in figure 4, such a film provides a continuous time record of the luminosity behind the slit. The motion of a luminous (or dark) pocket of gas from the injector toward the nozzle, for example, is resolved into an inclined line. For a given film velocity, the angle the streak makes on the film is a measure of the velocity of movement of the gas pocket.

Ion gaps. - Two ion gaps were mounted  $90^\circ$  apart at an axial station 7 inches from the injector face. Each gap was a conventional 18-millimeter single-gap spark plug. A 45-volt battery was placed in series with the gap and a 0.1 megohm resistor, and the voltage across the resistor was indicated on an oscilloscope. The plugs, which would withstand several seconds of normal operation, were severely eroded in a much shorter time during screaming operation.

#### Chamber Pressure Measurements

Pressure measurements of high-frequency transients were made with a Li-Liu pickup flush-mounted in the chamber wall about 3 inches from the injector wall. This pickup had a natural frequency of 28,000 cycles per second and a linear response to 1000 pounds per square inch pressure. The pickup was mounted in a steel chamber section which was substituted for the plastic section of the chamber.

## OPERATING PROCEDURE

Before the rocket engine was fired, the NACA high-speed camera was brought to normal operating speed. The rocket was then operated manually by the following procedure: automatic recording instruments and the moving-film camera were turned on; the acid control valve was opened; when entrance of acid into the chamber was observed, the fuel control valve was opened. Ignition was spontaneous with the furfuryl alcohol lead fuel. Flow regulation was obtained by presetting the control pressures to the pneumatically operated flow control valves.

At the onset of screaming combustion, which was audible and was visually evident by an intense brightening of the flame, the shutter of the NACA camera was tripped. Following this, the engine was shut down. Total running time ranged up to 8 seconds. The screaming combustion portion ranged from 1 to 3 seconds.

## PERFORMANCE

Because of the transient combustion effects encountered, performance was evaluated on the basis of thrust and flow values which existed approximately 0.7 second after ignition. This time corresponded approximately to the end of the furfuryl alcohol-JP fuel transition period and the beginning of the screaming combustion.

A plot of experimental specific impulse against oxidant-fuel weight ratio is shown in figure 5. The oxidant-fuel ratios for the screaming runs varied from 2.9 to 3.9. The two nonscreaming runs shown had oxidant-fuel ratios of 4.4 and 4.7. Inspection after these latter two runs revealed partial blocking of the injector orifices. Whether the nonscreaming combustion resulted from poor impingement or from the oxidant-rich mixture ratio is not known.

The maximum theoretical temperature of this propellant combination at a chamber pressure of 300 pounds per square inch has been calculated to be about 5275° R. In the oxidant-fuel ratio range where screaming occurred, the theoretical temperature is estimated to be about 4500° R. Therefore, the performance of 90 percent theoretical should result in an approximate chamber temperature of 3650° R.

## RESULTS AND ANALYSIS

The direct motion-picture photographs taken with the NACA 40,000-frame-per-second camera showed evidence of the rotary nature and frequency of the lateral oscillation. Streak-film records provided data for analysis of oscillation frequency and direction of wave and

propellant motion. Ion gaps confirmed the rotary analysis of the high-speed photographs, and pressure pickups provided measurement of the oscillation pressure strength. Erosion of the plastic chamber provided a relative indication of heat-transfer rates.

Qualitative impressions, such as the audible scream heard by the operator, also contributed to the over-all analysis of the screaming phenomena. For instance, the tone color of the scream varied from run to run. Some runs, those in which rotary oscillations occurred, emitted a clear intense note; screams in which rotary waves were not dominant were, in comparison, vapid and unclear.

The recording of combustion waves by direct photography creates a problem of interpretation. The luminosity of a wave in a combustible atmosphere may result from the combustion reaction, from thermal excitation in the wave front due to adiabatic compression, or from a combination of both. The light emission may or may not occur at the wave front; in this discussion, any time and position intervals between the actual pressure wave or wave front and the observed effects will be considered constant in order that the periods of oscillation and the estimated velocities may be considered unaffected.

#### Rotary Oscillation Shown by 40,000-Frame-Per-Second Photographs

The high-speed motion-picture photographs are illustrated in figure 6. Successive frames are printed in normal reading manner; the upper image of each frame is the top view ( $A_t$ ,  $B_t$ , etc.), and the lower image is the side view ( $A_s$ ,  $B_s$ , etc.). The injector is at the left of each image, and propellant flow is from left to right; propellant flow, when photographed at these rates, is too slow to be apparent in the frame-by-frame sequence and can be observed only when the sequence is illustrated as a motion picture. Likewise, the oscillations described in the next paragraph can be observed best by motion-picture presentation.

The bright and dark parts of each image shift from frame to frame. If the path of the bright zone is followed, frame by frame, for both the top and side views, it will be apparent that the bright zone generally moves from side to side in a cyclic manner. The cyclic motion is illustrated as a line diagram in figure 7, which shows a short sequence of figure 6.

It is immediately apparent that the respective motions of the bright zones are out of phase. Thirty-three cycles of figure 6 were analyzed and the phase displacements between the top and side views were found to be consistently in one direction and to average about  $85^\circ$ . The effect of image distortion due to the lens effect of the thick chamber walls was minimized by considering reference positions for the phase measurement

at the sides of the cylinder. The slight deviation from  $90^\circ$  phasing is probably due to the approximately  $6^\circ$  angular displacement of the top view mirror. The only probable motion that satisfies the described cycling and phasing is rotary. No implication is intended that combustion existed only in the bright areas; the preceding analysis depends solely upon the existence of a combustion disturbance that showed cycling and a phase difference in the two views.

A cyclic brightening is apparent in both views of the chamber. Study of the brightest frames reveals that these occur when the luminous zone is on the near side of the chamber. Attenuation of light in the other frames is probably due to absorption by the chamber gases.

The average frequency of the rotary oscillation was measured in the sequence of figure 6 as 5200 cycles per second. This frequency can be compared with the acoustical frequencies for the transverse modes of a cylindrical chamber which are given by the equation (ref. 8)

$$f = c\beta/2r$$

where  $c$  is the acoustic velocity,  $r$  is the chamber radius, and  $\beta$  has the following values for the first few transverse modes:

Tangential order	$\beta$	Radial order	$\beta$
1	0.586	1	1.220
2	0.972	2	2.233
3	1.337		

The rotary motion of the luminous zone in the rocket chamber corresponds most closely to the rotating wave form of the first tangential transverse mode. For this mode,  $\beta$  is 0.586 and is, of course, independent of whether the wave is a standing wave system (sloshing mode) or a rotating wave as observed in the motion pictures. If an acoustical velocity of 3675 feet per second is assumed, corresponding to the maximum theoretical flame temperature of  $5275^\circ\text{R}$ , the calculated maximum frequency is 6460 cycles per second.

The lower observed frequency of 5200 cycles per second may be explained in either of two ways: the observed frequency corresponds to a chamber temperature of only  $3400^\circ\text{R}$  and a velocity of 2960 feet per second; alternatively, the observed frequency may correspond to a combination of lateral and longitudinal modes of oscillation.

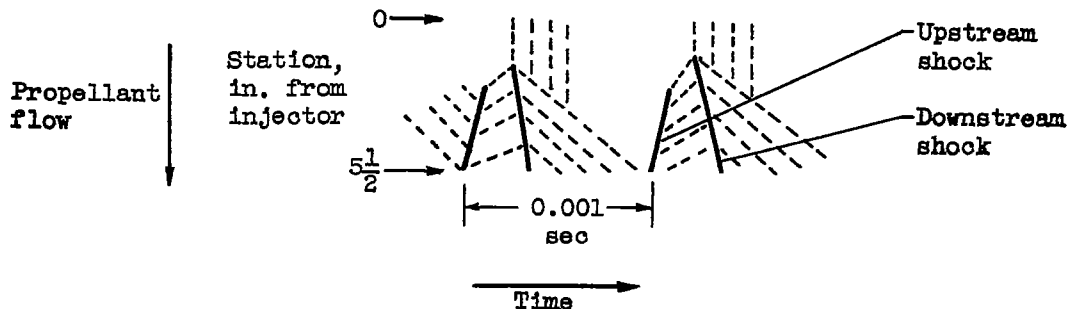


## Oscillations Recorded by Streak Photography

The streak photographs provided data for analyzing propellant flow velocities, pressure wave velocities, and oscillation frequencies. Figures 8, 9, and 11 are records of the luminosity behind the slit where the transparent section was located adjacent to the injector. Figure 10 shows streak photographs near the nozzle.

Smooth propellant flow is illustrated by figure 8(a) and occurred during flow of the starting slug of furfuryl alcohol. During smooth flow, the first 2 inches of the chamber remained dark. The first luminous streak indicates a gas velocity of about 80 feet per second, which is approximately the propellant jet injection velocity. The apparent gas velocity at station  $5\frac{1}{2}$  is approximately 400 feet per second. The theoretical gas velocity in the chamber based on maximum flame temperature at 90 percent maximum specific impulse would be 360 feet per second.

Figures 8(b) and 8(c) show periodic fluctuations of luminosity that increased in intensity to become well-defined longitudinal shocks in figure 8(d) in about 0.02 second. The occurrence of this transition from smooth burning to longitudinal shock occurred approximately during the transition from furfuryl alcohol to JP-3 fuel. The frequency of the earlier fluctuations was about 900 cycles per second. The frequency increased to approximately 1000 cycles per second when the shocks occurred, which are illustrated here in a sketch.



The slightly increased frequency during shock oscillation may be due to increased wave strength, to increased average chamber temperature from more efficient combustion, or to both.

The acoustical frequency of the longitudinal mode of oscillation may be calculated from the simplified equation

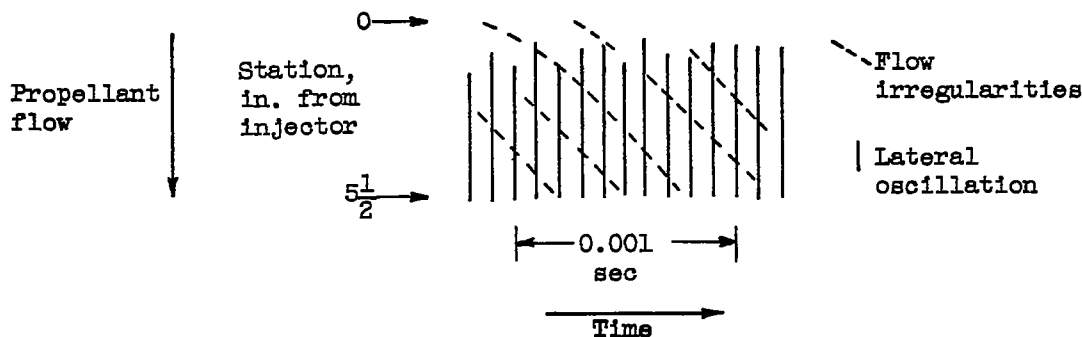
$$f = nc/2l$$

For an acoustical velocity  $c$  of 3675 feet per second (based on maximum temperature of  $5275^{\circ}\text{R}$ ) and a length  $l$  of 20.5 inches (to the start of the converging section), the acoustical frequency of the first (harmonic order,  $n = 1$ ) longitudinal oscillation should be 1075 cycles per second. If the observed frequency of 1000 cycles per second were used as a basic

parameter, the acoustical velocity would be 3415 feet per second and the average chamber temperature would be 4520° R.

Since the downstream shock moves with the gas flow and the upstream shock moves against the gas flow, the apparent velocities relative to the chamber wall are different (respectively, 3900 and 3150 ft/sec), as evidenced by the different slopes of the shock lines. However, the shock velocities relative to the gas were nearly identical, and the velocity averaged 3500 feet per second.

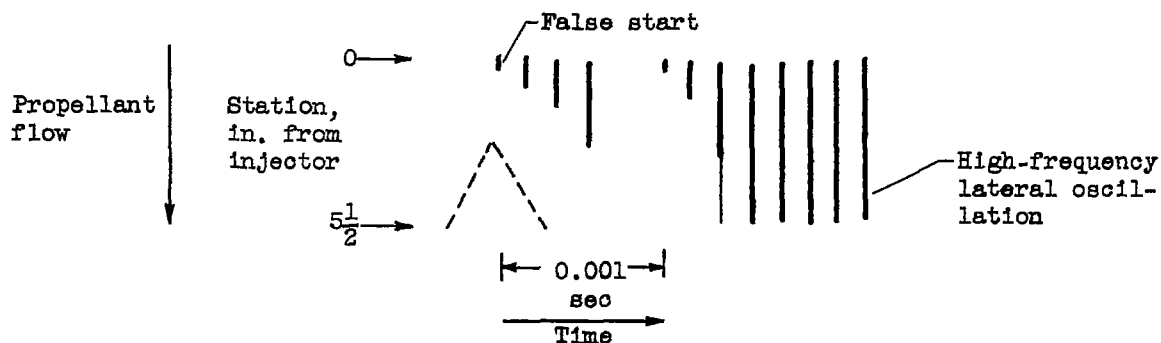
During the interval of longitudinal shock generation, a lateral oscillation (faint vertical lines) with an apparently uniform frequency of approximately 10,000 cycles per second also appeared, as shown in figures 8(b) and 8(c). Because the faint lines are barely discernible in the original photographs and therefore difficult to reproduce, the oscillations are emphasized in the sketch.



This oscillation varied slightly in intensity and persisted for about 0.03 second. The fact that the traces are vertical means that the entire window slit was illuminated at one time, and therefore that the oscillation probably had no longitudinal component.

If the acoustical velocity of 3415 feet per second (computed from observed longitudinal oscillation frequency of 1000 cycles/sec) is assumed, the lateral oscillation of 10,000 cycles per second reveals that  $\beta$  is 0.976. This agrees with the second tangential mode in which  $\beta$  equals 0.972.

A more prominent series of vertical lines indicated other lateral oscillations, as shown by figures 8(e) and 8(f).



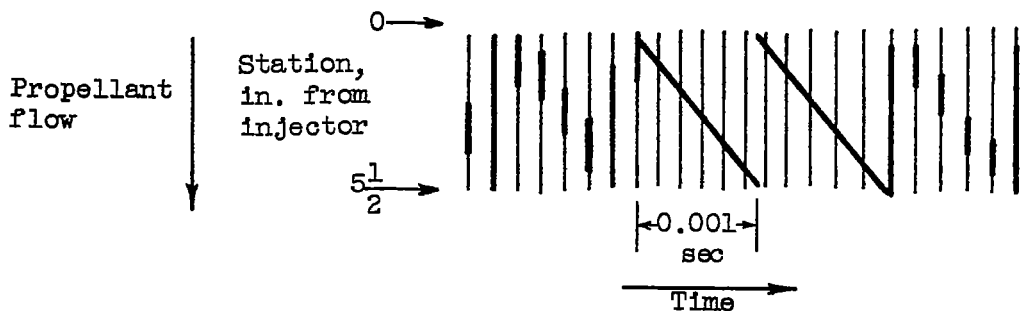
After several "false starts" as indicated by the short vertical lines, the lateral oscillations showed an impressively increased brilliance along the entire length of the window. The period of oscillation corresponded to a frequency of approximately 6000 cycles per second. The frequency attained a maximum value within a few cycles and gradually diminished during part of the run to an average value of about 5800 cycles per second. Once started, the lines of the strong lateral oscillation persisted throughout the remainder of the run. The earlier lateral oscillations of 10,000 cycles per second and the later lateral oscillations of 6000 cycles per second were so distinctly different in luminosity, as well as frequency, that different modes of oscillation are probably signified.

In the streak photographs, the frequency and the apparent lateral nature of the oscillation correlate closely with the rotary oscillation indicated by the 40,000-frame-per-second photographs; presumably the lateral oscillations of 6000 cycles per second in the streak photographs were also rotary. If this lateral oscillation of 6000 cycles per second is assumed to have an acoustical velocity of 3415 feet per second corresponding to the computed velocity from longitudinal frequencies,  $\beta$  has a value of 0.586. This also agrees well with the first tangential mode in which  $\beta$  is theoretically 0.586.

Figure 9 is similar to the sequence of figure 8 except that the phenomena occurred in a shorter time interval. Figure 9(a) is smooth combustion. The cyclic fluctuations, illustrated in figure 9(b), increased to strong longitudinal shock waves in only 0.008 second, as seen in figure 9(c). The high-frequency lateral oscillations at 10,000 cycles per second, evident in another run in figures 8(b) and 8(c), are apparently missing. The "false starts" of the lower frequency lateral oscillation are distinct in figure 9(c), and the onset of continuous strong lateral oscillation evidently caused excessive strain on the chamber. The chamber cracked in less than 22 lateral cycles, as indicated by the explosive whitening of the entire film.

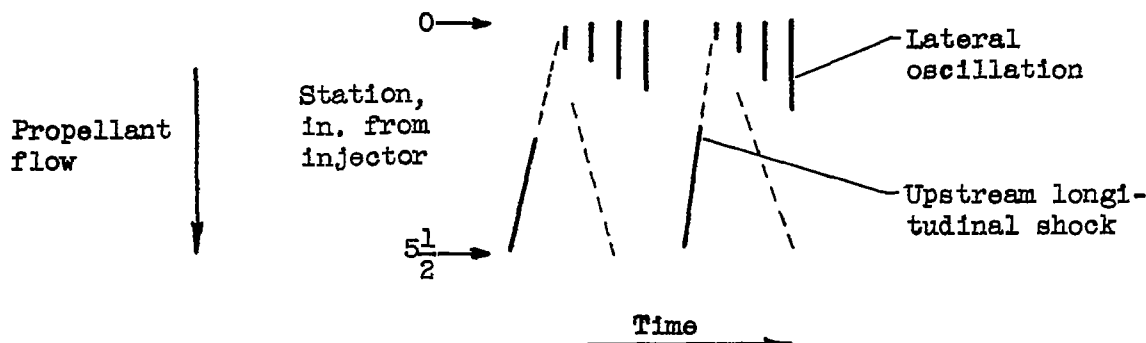
The combustion and oscillation phenomena near the nozzle end of the chamber were similar to those near the injector. Figure 10(a) shows smooth combustion with a gas flow velocity at station  $16\frac{1}{2}$  of about 425 feet per second. The longitudinal oscillations at approximately 1000 cycles per second showed the usual shock line discontinuities as illustrated in figure 10(b). An extrapolation of the upstream and downstream shocks to intersect each other indicates an effective acoustical chamber length of 21.5 inches, which corresponds approximately to the distance to the midpoint of the convergent section of the nozzle. This measurement and the previous value of measured shock wave velocities and longitudinal oscillation frequency are consistent and agree remarkably well with the theoretical calculations.

The lateral oscillations were also evident near the nozzle, as shown by figure 10(c). The lateral oscillations and the longitudinal oscillations usually existed simultaneously. In figures 8(e) and 8(f), the longitudinal oscillations are indicated by the cyclic, bright diagonal



zones of propellant flow. These diagonals have a frequency of about 1000 cycles per second. In figures 10(c) and 10(d), the longitudinal waves are indicated by dark zones, also at about 1000 cycles per second. The shock lines of the longitudinal wave, missing in figure 10(c), actually become discernible again in figure 10(d) but are more clearly defined in figures 10(e) and 10(f). Sometimes the lateral oscillations are dominant, and other times the longitudinal modes are dominant; no strength interrelation seems apparent.

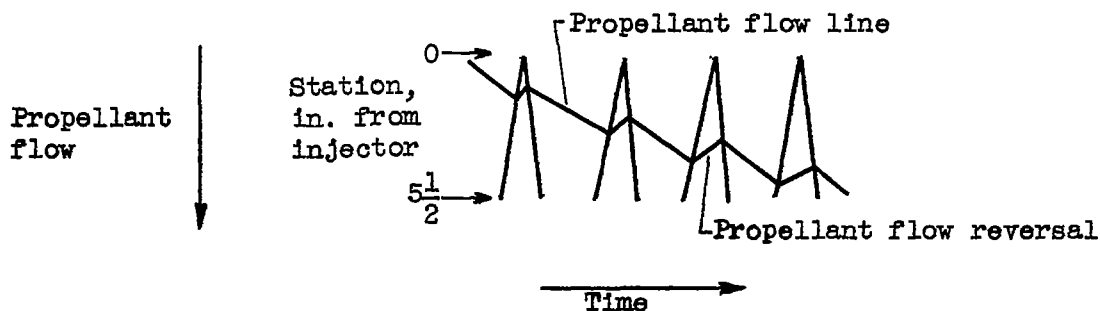
In general, the ratio of the frequencies of the lateral oscillations to the longitudinal oscillations varied during the course of a run from  $4\frac{1}{2}$  to 6. Since no fixed ratio exists between the frequencies, the oscillation modes appear to be acoustically independent of each other. However, this statement is not intended to imply that one mode of oscillation is without effect on the other, and the possibility of some form of interdependence of oscillations is shown in figures 8(d) and 9(c). The reflection of the upstream longitudinal wave at the injector wall



apparently stimulates, triggers, or initiates the lateral oscillation, which at first vanishes in a few lateral cycles only to restart at the next reflection of the longitudinal wave. In future work, the relation of this triggering action may be effectively studied by suitably placed baffles or grids near the injector. In any case, the effect of grids or other baffles on damping the reflections will help to establish the character of the oscillations.

An interaction is also indicated in figure 10(d), where the lateral oscillations appear to be influenced by the passage of the longitudinal waves and the slopes of the lateral lines tend to parallel the longitudinal shock lines.

Combined lateral and longitudinal variations are illustrated by several examples in figure 11. Each of the narrow inverted vertical V's appears to comprise two waves joined at the injector. The deviation of



the waves from the vertical indicates a longitudinal component in the lateral wave. The average frequency of 4200 cycles per second is similar to the frequency of the lateral oscillations previously discussed. The absence of any periodic changes resembling the longitudinal frequency of 1000 cycles per second indicates that the fundamental longitudinal wave is not present. However, the propellant flow lines show a discontinuity in zig-zag fashion that resembles flow reversal during the passage of the lateral wave. The flow reversal would indicate that the lateral wave had a longitudinal component.

The frequency of these oscillations varied irregularly from 4000 to 5000 cycles per second and seemed greatest when the magnitude of the longitudinal velocity component was greatest; that is, when the line of the lateral wave was most nearly vertical. The apparent velocities of propagation in the longitudinal direction vary for the waves shown in figure 11 from an estimate of 9000 feet per second to an infinite velocity (vertical trace). This is contrary to the hypothesis that these waves may be due to a combined lateral and longitudinal mode. The acoustical frequency of such a combined mode is given by the equation

$$f = c/2 \sqrt{(\beta/r)^2 + (n/l)^2}$$

The equation indicates that the oscillation frequency for a combined mode is greater than the frequency for either a pure transverse or longitudinal mode of corresponding order.

Lack of a fixed relation between the longitudinal velocity component of the wave and the frequency of the lateral component makes any analysis uncertain.

#### Ion Gap Traces

The ion gap probes proved unable to withstand the extremely high heat transfer under screaming combustion conditions. However, some indication of a rotating pressure wave is shown in figure 12. The two upper traces are calibration traces of a 5000-cycle-per-second oscillation impressed simultaneously on each probe. The two lower traces are ion gap voltage changes of run 2, with the two probes geometrically spaced 90° apart and each probe at an axial station 7 inches from the injector face.

The analysis shows a cycling frequency of about 6300 cycles per second, with an average angular displacement of about 105°. The high frequency of 6300 correlates closely with the initial frequency of about 6000 cycles per second shown in figure 8(e).

#### Pressure Measurements

Reproductions of pressure records taken during a run in which screaming occurred are shown in figure 13. The pressure detector was mounted at a position corresponding to the center of the upstream transparent section, except, of course, that the plastic was replaced by a steel section tapped for the pickup. Although not made in the same run the pressure records correlate with the streak-film records shown in figures 8 and 9.

The build-up of the longitudinal oscillations to shock-fronted waves is shown in figure 13(a). The shocks are clearly indicated at the right of this strip. Two shocks per cycle are shown; the first was evidently the upstream moving shock and the second was its reflection from the injector face (compare with fig. 8(b)). The indicated pressure across the first shock rose from 225 pounds per square inch to 450 pounds per square inch, a pressure ratio of 2; across the second shock the pressure rose from 350 pounds per square inch to 640 pounds per square inch, a pressure ratio of about 1.8. The ratio between maximum and minimum chamber pressure during a cycle was 2.8.

Pressure traces after the development of the 5000-cycle oscillation are shown in figure 13(b). The presence of the longitudinal mode oscillation is evident in the periodic rise and fall of 100 pounds per square inch amplitude in the crests of the pressure peaks. The natural frequency of the pickup (28,000 cps) confused the record somewhat and it is difficult to ascertain whether the lateral oscillations were shock-fronted. For an average cycle the indicated pressure varied from a minimum of 210 pounds per square inch to a maximum of 870 pounds per square inch, a pressure rise ratio of about 4.2.

#### Plastic Chamber Erosion

The plastic section of the combustion chamber eroded faster under screaming combustion than under normal smooth combustion. In addition, the strong clear scream occurred with strong rotary oscillation and with the highest erosion rates; the vapid screams accompanied oscillations which were predominantly longitudinal and which had lower erosion rates.

Figure 14 is a plot of radial erosion rates for several axial stations of the plastic section. The erosion of the plastic during rotary screaming combustion was quite uniform circumferentially, and the erosion rate at each station was rather uniform with some tendency toward a slightly increased rate at stations progressively closer to the injector. On the other hand, screaming combustion without rotary oscillation showed similar uniformly concentric erosion rates but with a decreased rate of erosion toward the injector. Smooth combustion showed definitely non-uniform erosion rates concentrically and axially.

All the erosion rates were computed as averages - total erosion divided by seconds of running time. The smooth portion of each screaming run (time and extent of erosion) was subtracted from the total to obtain a more realistic average erosion rate.

The rotary mode of oscillation caused average erosion rates six times that of smooth combustion, which is plotted as reference. Erosion during predominantly longitudinal mode screaming was about three times

3168

the smooth combustion erosion rates. Although the erosion rates of the plastic chamber indicated an appreciable increase of heat transfer during longitudinal screaming, the most severe transfer occurred during rotary screaming.

The rotary disturbance was probably accompanied by boundary layer changes at the cylinder wall as a result of either a decrease in the effective laminar boundary layer thickness or an increase in turbulence or both. The reduction of boundary layer thickness would substantially increase the temperature gradient; the turbulence would cause macroscopic gas transfer to the wall. Either condition could contribute to high heat transfer to the wall.

From these measured erosion rates it can be postulated that the rotary mode of oscillation is more conducive to engine failure than the longitudinal mode. During one of the intense screaming runs of about  $3/4$  second, the injector face was seriously eroded and the pattern of erosion indicated a tangential outward swirl. A photograph of the eroded injector is shown in figure 15.

#### DISCUSSION

The modes of oscillation observed in these experiments have been previously studied by other investigators. Smith and Sprenger (ref. 9) conducted an extensive investigation of rotary transverse waves in solid propellant rocket engines. There are numerous instances of damage to injectors and scorch patterns in the chamber walls which have indicated the existence of spinning oscillations in liquid-propellant rocket engines (ref. 10).

The screaming frequencies recorded with this engine have been shown to correlate with simple acoustical modes of the chamber. The observed frequencies were consistently somewhat lower than the frequencies calculated from theoretical temperature for the corresponding acoustical mode because the mean chamber temperature is logically always less than the theoretical flame temperature for maximum specific impulse.

Because of the correlation of observed screaming frequencies and acoustical modes of oscillation, screaming has been considered to be an acoustical oscillation driven by combustion that is accelerated during the high pressure part of the cycle, in accordance with the Rayleigh principle (ref. 11). A number of fundamental papers on studies of heat-driven acoustical oscillations have been issued. Reference 5 discusses the influence of propellant through-flow on the oscillations. References 12, 13, and 14 give results of oscillations of relatively low amplitude studied in burner-tube experiments; this is in contrast with the severe oscillations observed in the rocket engines.



The streak photographs and the pressure measurements in this report indicate that the pressure waves in a rocket engine during fully developed screaming are strong waves of pressure ratios 2 to 4 and that the longitudinal waves, at least, have distinct shock fronts. In the case of rotary or transverse waves there may be considerable doubt that shock fronts are developed; strong waves of large pressure ratios may exist in such a two-dimensional field (the cross section of the chamber) without developing distinct wave fronts. Neither the streak photographs nor the pressure measurements are sufficiently clear to settle this question.

In seeking the combustion mechanism which sustains rocket screaming, one must survey a number of observations. Evidently the pressure disturbances accelerate the combustion reactions, and the combustion reactions, in turn, sustain the pressure waves. Not all the unburned propellant is necessarily consumed behind each pressure wave; it is more likely that, in a rocket chamber where the combustion environment is heterogeneous and the propellants are incompletely mixed, the reaction set off by the passage of a pressure wave consumes only that part of the propellant mixture vaporized and within a combustible range. The turbulence and heat caused by the passage of the shock front and by the combustion wave immediately after the front induce increased vaporization and mixing in the unreacted portion of the charge, which then is susceptible to "triggering" by a succeeding pressure wave. Thus a particular pocket of propellant mixture may augment or drive each of several waves. It is apparent that augmentation of pressure waves does not demand ignition of unburned charge but merely acceleration of the burning rate.

It has been suggested (refs. 9, 10, and p. 30 of 15) that the combustion mechanism may be related to detonation, that is, a shock-fronted pressure disturbance that ignites unburned propellant and derives its energy from the trailing conflagration. The qualitative agreement of the detonation definition with the observations of screaming combustion and the observed destructiveness of screaming make a detonation-like mechanism reasonable. However, the pressure ratios and wave propagation velocities observed in rocket engines are much less than those for detonation of premixed charges in confining tubes; this may be due to partial reaction as previously discussed. Two other factors stand out: (1) The transverse oscillations may not be shock-fronted, and (2) the pressure wave may merely accelerate rather than initiate combustion. For these reasons the term detonation may not be an accurate description of the reaction mechanism of screaming.

Before fully developed screaming occurs, both the streak photographs and the pressure records indicate that the longitudinal oscillations are generated from initially weak (acoustical) oscillations. In contrast, the lateral oscillations appear in these records to be initiated by previous strong longitudinal oscillations. Weak oscillations are presumably present in the chamber even during normal combustion, possibly

as decaying reverberations of random combustion pulses. The combustion reaction mechanism is apparently sensitive to even these relatively weak pressure waves and is sufficiently rapid to reinforce them. To accord with the Rayleigh principle, the combustion "time delay" must be less than 0.00005 second (1/4 cycle) to reinforce a 5000-cycle-per-second oscillation. For these weak waves the term detonation seems inappropriate.

Although the data presented in this report do not establish the mechanism supporting the screaming oscillations, it appears that a coupling of strong wave reflection phenomena in the chamber with a pressure-sensitive heat release mechanism is necessary to explain the observed effects. Further fundamental combustion studies under the high pressure conditions of rocket combustion and studies of techniques for attenuating strong pressure reflections within the chamber are needed to predict and control screaming in rocket engines.

#### SUMMARY OF RESULTS

A photographic investigation of combustion-driven oscillations in a 1000-pound-thrust acid-jet fuel rocket engine equipped with a transparent section and operating at 300 pounds per square inch chamber pressure has revealed the following information:

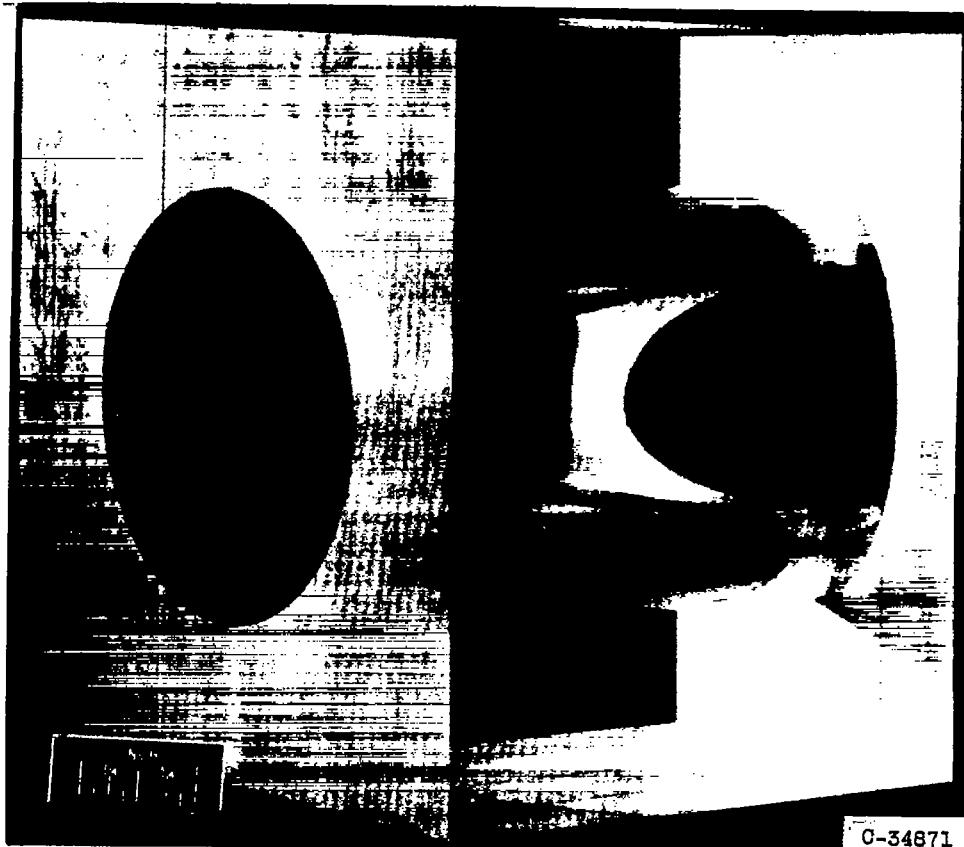
1. Oscillations with frequencies of roughly 1000 and 4000 to 6000 cycles per second were observed. The frequency of the 1000-cycle-per-second oscillation can be correlated with the longitudinal acoustical mode; the 6000-cycle-per-second frequency can be correlated with the first transverse tangential mode. The 40,000-frame-per-second pictures taken with two views show that the 6000-cycle-per-second oscillation is the rotating wave form of the transverse tangential wave; that is, the wave front rotates around the periphery of the chamber.
2. Pressure measurements along the wall of the chamber indicated that the longitudinal waves formed shock fronts with pressure ratios before and after the shock of roughly 2, and a ratio of nearly 4 between maximum and minimum chamber pressure at different times in a cycle. For the rotary waves, pressure ratios of roughly 4 between maximum and minimum chamber pressure were observed with instantaneous maximum chamber pressures near 900 pounds per square inch.
3. Based on the erosion of the plastic section of the chamber, the heat-transfer rate when longitudinal oscillations were present was about twice that for normal combustion and about six times normal when both rotary and longitudinal oscillations were present.

Lewis Flight Propulsion Laboratory  
National Advisory Committee for Aeronautics  
Cleveland, Ohio, February 2, 1954

## REFERENCES

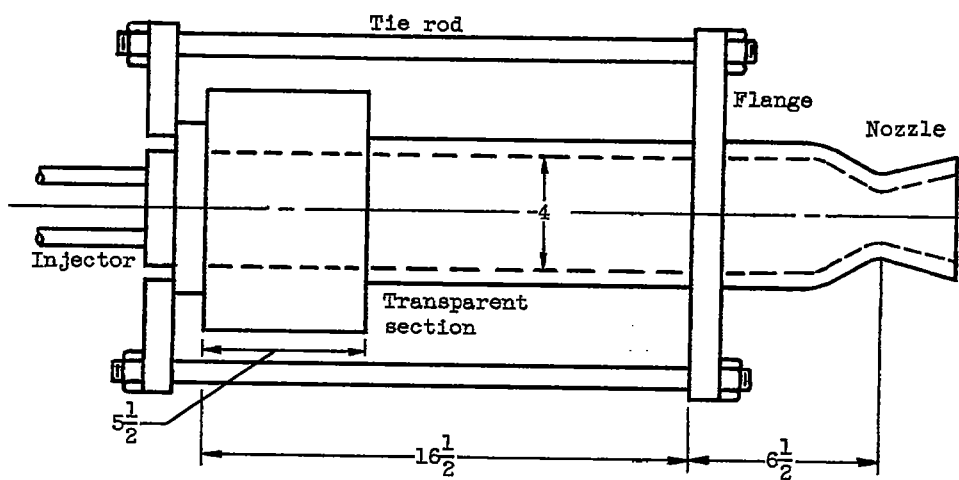
1. Ellis, Herbert, Odgers, Irving, Stosick, A. J., Van De Verg, N., and Wick, R. S.: Experimental Investigation of Combustion Instability in Rocket Motors. Fourth Symposium (International) on Combustion, The Williams & Wilkins Co., 1953, pp. 880-885.
2. Tischler, Adelbert O., Massa, Rudolph V., and Mantler, Raymond L.: An Investigation of High-Frequency Combustion Oscillations in Liquid-Propellant Rocket Engines. NACA RM E53B27, 1953.
3. Berman, Kurt, and Cheney, Samuel H., Jr.: Combustion Studies in Rocket Motors. Jour. Am. Rocket Soc., vol. 23, no. 2, Mar.-Apr. 1953, pp. 89-95; discussion, pp. 96-98.
4. Bragdon, Thomas A., Lewis, George D., and King, Charles H.: Interim Report on Experimental Investigation of High Frequency Oscillations in Ramjet Combustion Chambers. M.I.T. Meteor Rep. UAC-53, Res. Dept., United Aircraft Corp., Oct. 1951. (BuOrd Contract NOrd 9845.)
5. Blackshear, Perry L., Rayle, Warren D., and Tower, Leonard K.: Experimental Determination of Gas Motion Accompanying Screeching Combustion in a 6-Inch Simulated Afterburner. NACA RM E53I28, 1953.
6. Harp, James L., Jr., Vêlie, Wallace W., and Bryant, Lively: Investigation of Combustion Screech and a Method of Its Control. NACA RM E53L24b, 1954.
7. Miller, Cearcy D.: The NACA High-Speed Motion-Picture Camera. Optical Compensation at 40,000 Photographs Per Second. NACA Rep. 856, 1946. (Supersedes NACA ACR E6C25.)
8. Morse, Philip M.: Vibration and Sound. Second ed., McGraw-Hill Book Co., Inc., 1948.
9. Smith, R. P., and Sprenger, D. F.: Combustion Instability in Solid-Propellant Rockets. Fourth Symposium (International) on Combustion, The Williams & Wilkins Co., 1953, pp. 893-906.
10. Anon.: Development of AJ11-9 Liquid-Propellant Booster Rocket. Rep. No. 611, Apr. 1, 1951-Mar. 31, 1952, Aerojet Eng. Corp., Nov. 20, 1952. (Boeing Subcontract, U.S. Air Force Contract AF33(038)-19589, Proj. MX-1599.)
11. Rayleigh: The Theory of Sound. Vol. II. Dover Pub., 1945, pp. 232-234.

12. Putnam, Abbott A., and Dennis, William R.: Low-Frequency Oscillations in a Flame-Filled Tube. Tech. Rep. No. 15034-1, Battelle Memorial Inst., May 1953. (Contract No. AF 33(038)-12656, E.O. No. 460-35 S.R.-8.)
13. Putnam, Abbott A., and Dennis, William R.: Burner Oscillation of the Gauze-Tone Type. Tech. Rep. No. 15034-2, Battelle Memorial Inst., Aug. 1953. (Contract No. AF 33(038)-12656, E.O. No. 460-35 S.R.-8.)
14. Putnam, Abbott A., and Dennis, William R.: Suppression of Burner Oscillations by Acoustical Dampers. Tech. Rep. No. 15034-3, Battelle Memorial Inst., Aug. 1953. (Contract No. AF 33(038)-12656, E.O. No. 460-35 S.R.-8.)
15. Anon.: Combined Bimonthly Summary No. 36, Apr. 20-June 20, 1953. Jet Prop. Lab., C.I.T., July 20, 1953.



C-34871

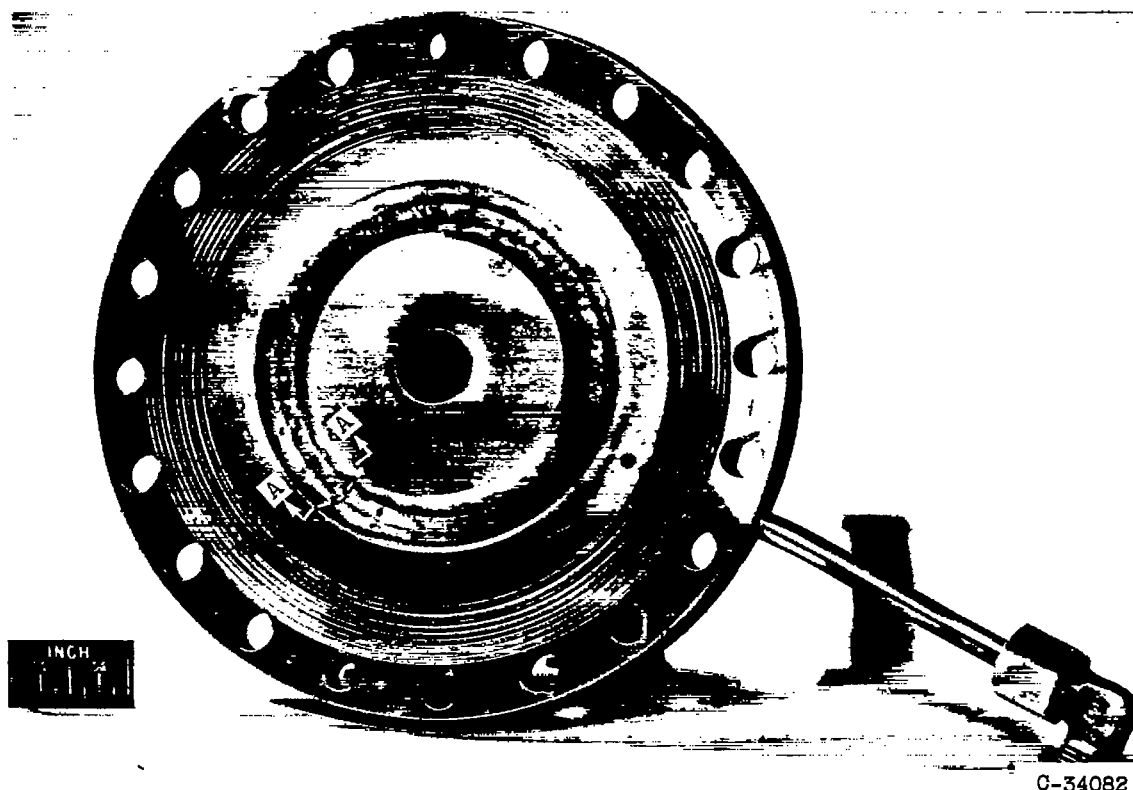
(a) Transparent chamber section.



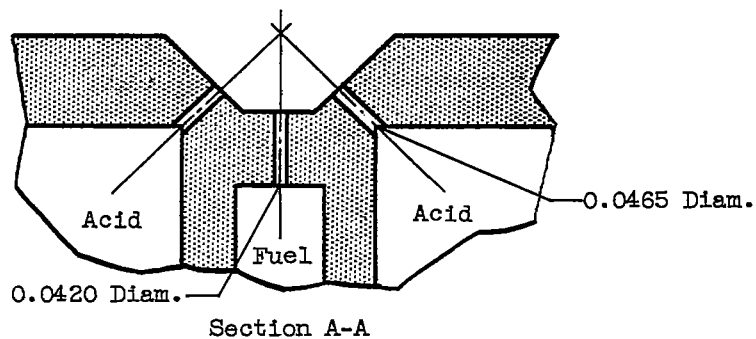
(b) Rocket assembly.

Figure 1. - Rocket engine with transparent chamber section.

3168



Annular triplet-impingement injector



Cross section of one set of propellant orifices. Injector ring contains 24 sets of orifices.

Figure 2. - Annular triplet-impingement injector for 1000-pound acid-hydrocarbon rocket engine.

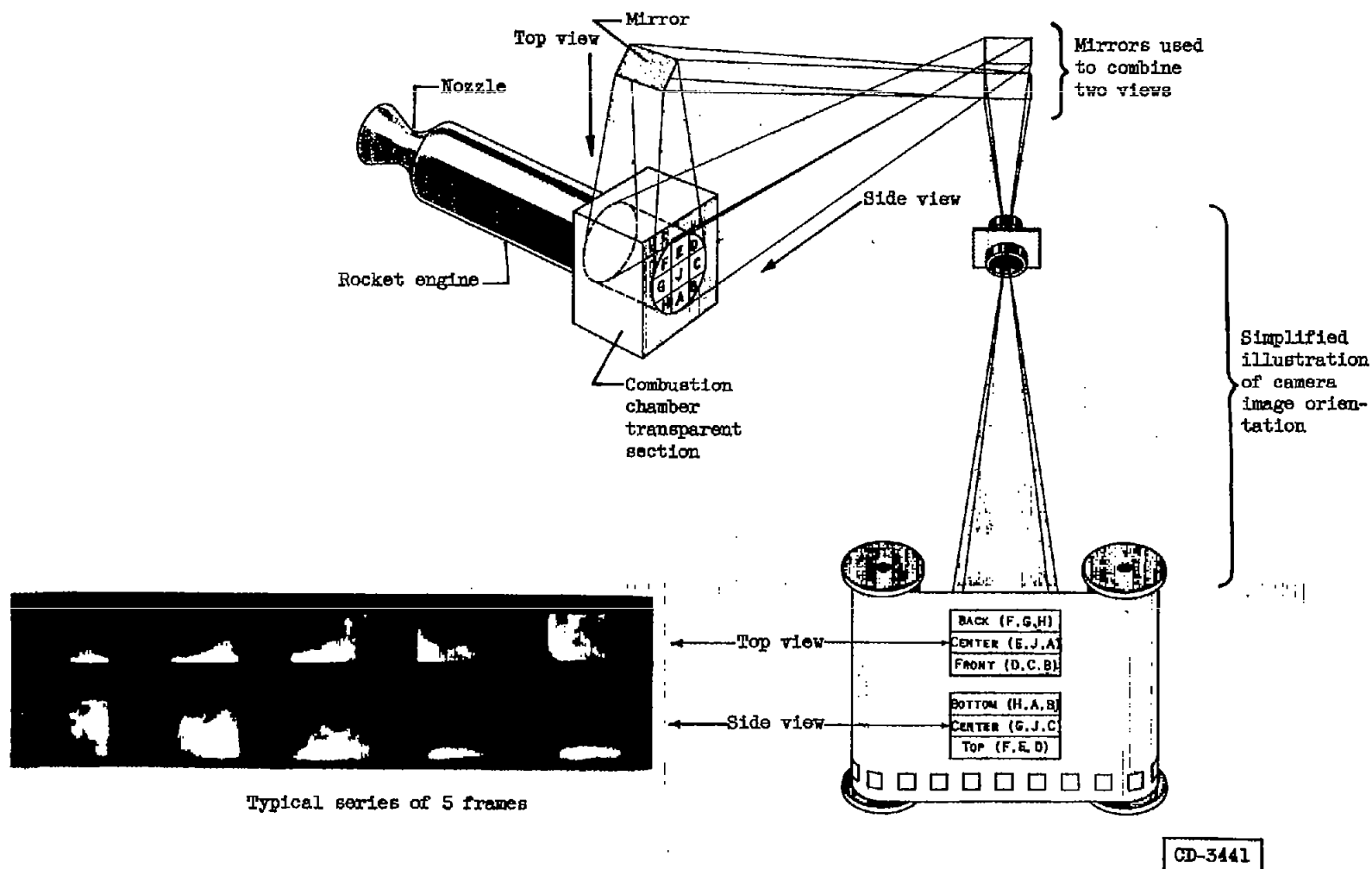


Figure 3. - Schematic illustration of optics used with NACA 40,000-frame-per-second camera. Both views of chamber recorded simultaneously. Letters indicate injector end of axial sections.

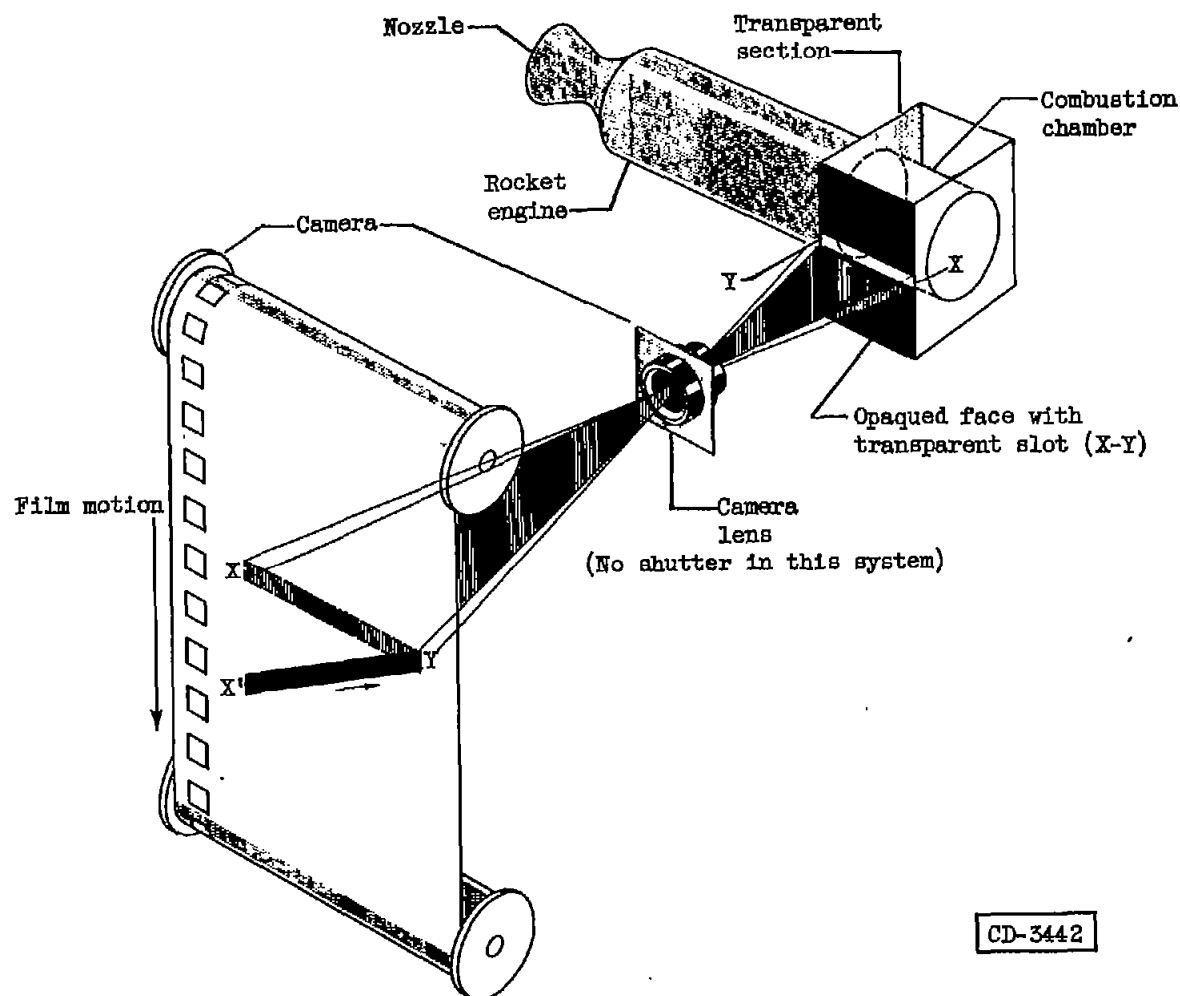


Figure 4. - Schematic illustration of optics of moving-film streak photography. If, during movement of continuous film, a bright light moves in rocket engine from X to Y, a diagonal line X'Y (resultant of combined film and bright light motions) will be traced on film.



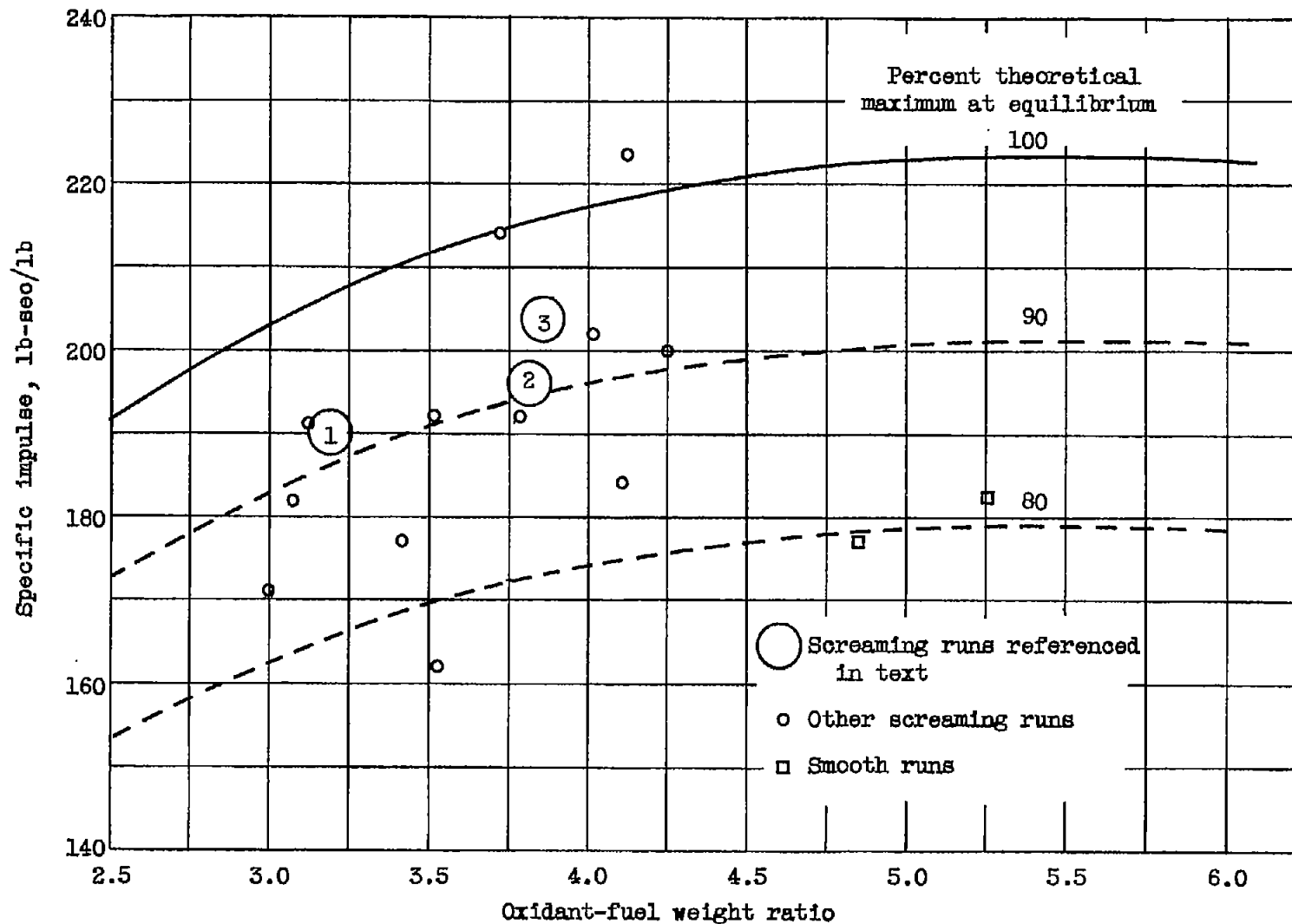
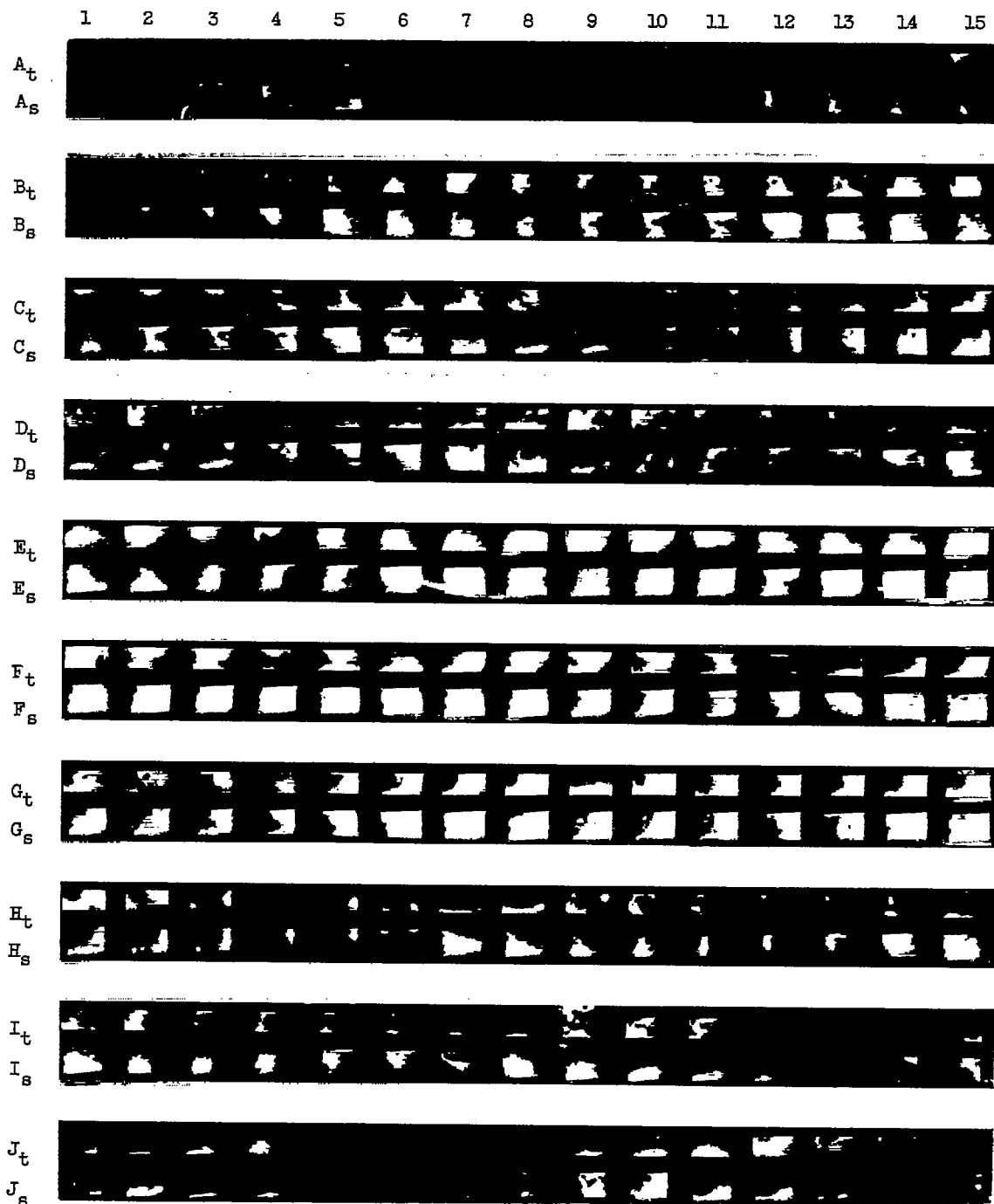


Figure 5. - Performance of 1000-pound-thrust rocket engine with WFNA and JP-3 fuel.



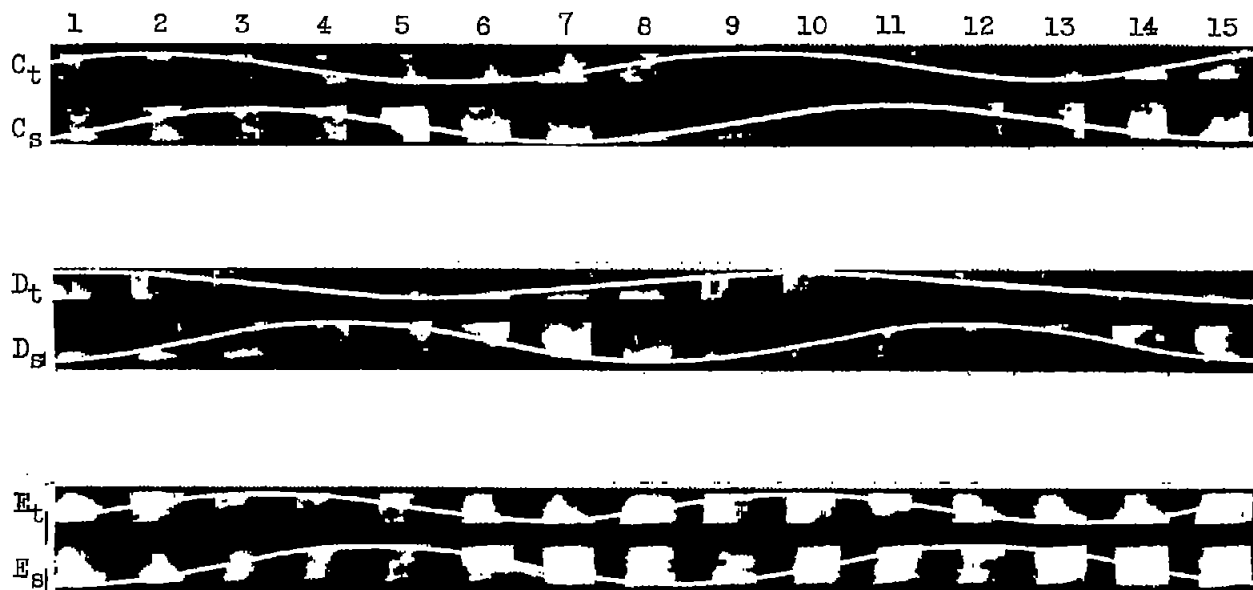
C-33524

Figure 6. - Rotary combustion oscillation in 1000-pound-thrust rocket engine with WFNA and JP-3 taken at 42,000 frames per second for run 1.



C-33525

Figure 6. - Concluded. Rotary combustion oscillation in 1000-pound-thrust rocket engine with WFNA and JP-3 taken at 42,000 frames per second for run 1.



C-33524

Figure 7. - Tracing of motions of luminous zone for determining frequency and phase relations of rotary oscillation of 42,000-frame-per-second sequence. Run 1; lines C, D, E of figure 6.

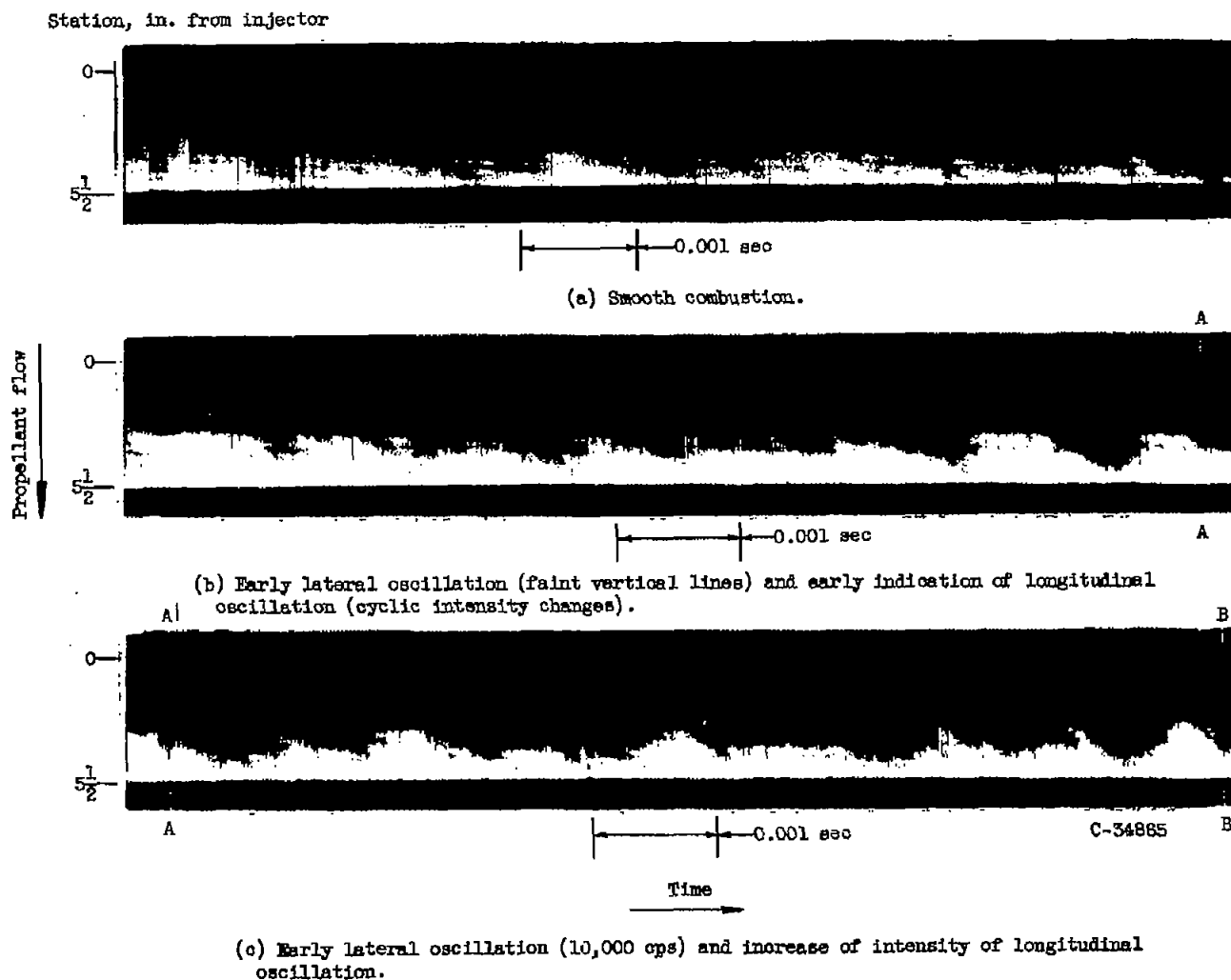
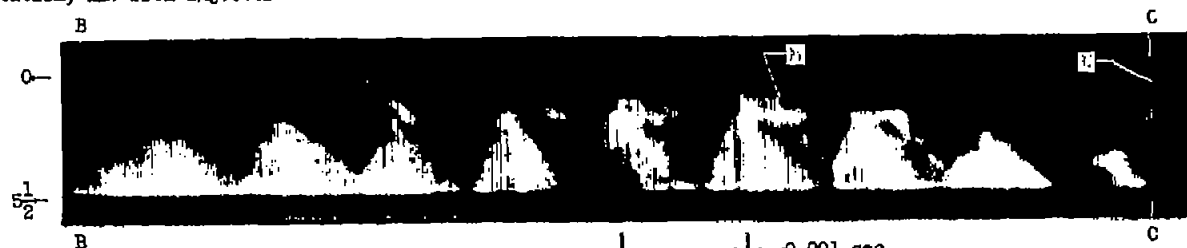


Figure 8. - Streak photographs showing oscillations between stations 0 and  $5\frac{1}{2}$  of screaming combustion in a 1000-pound-thrust rocket engine with WFMA and JP-3 for run 2.

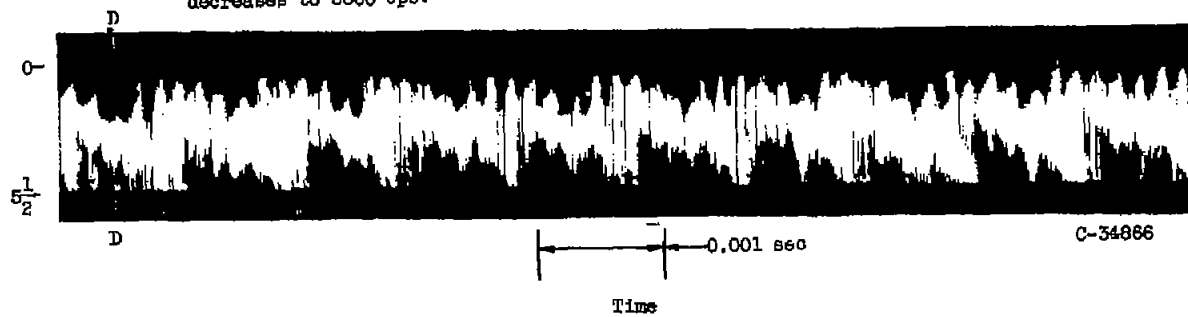
Station, in. from injector



(d) Increase of longitudinal oscillation to strong longitudinal shock. Lateral oscillation ( $M$ , 8000 cps) in early stages degenerates to start of strong lateral oscillation ( $N$ , 4600 cps).



(e) Intense lateral oscillation (full intense vertical lines) starts at 6000 cps and decreases to 5800 cps.



(f) Diagonal bright zones indicate longitudinal oscillation (1000 cps) superimposed on lateral oscillation (5800 cps).

Figure 8. - Concluded. Streak photographs showing oscillations between stations 0 and  $5\frac{1}{2}$  of screaming combustion in a 1000-pound-thrust rocket engine with WNA and JP-3 for run 2.

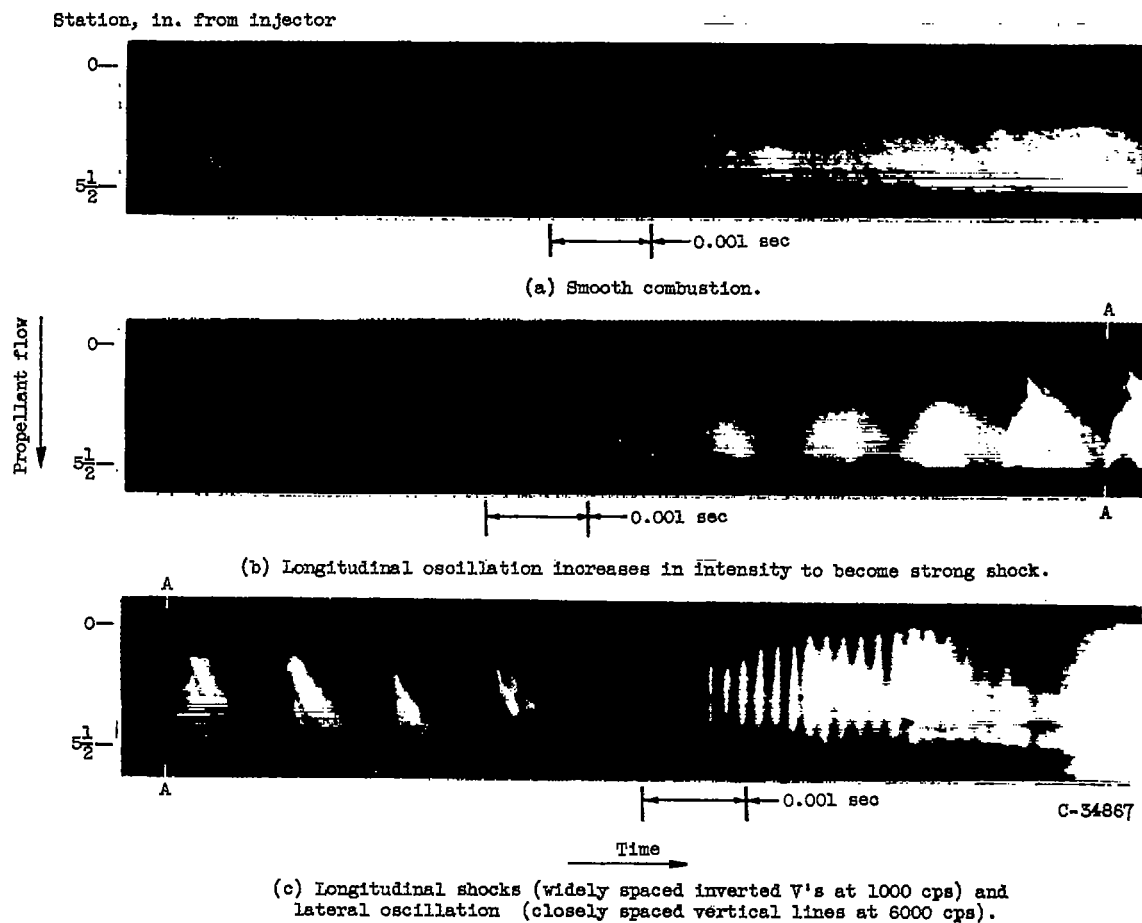
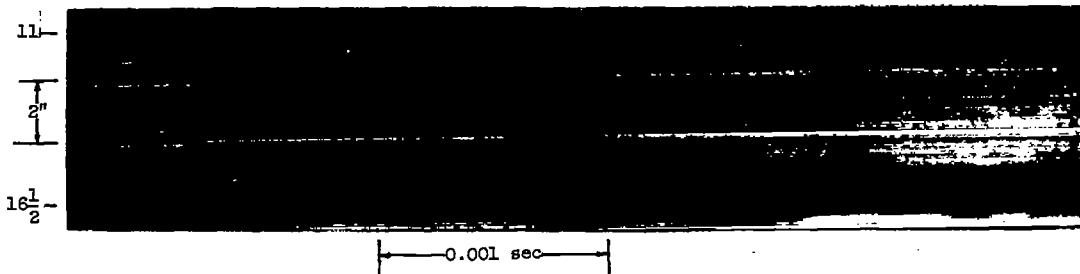
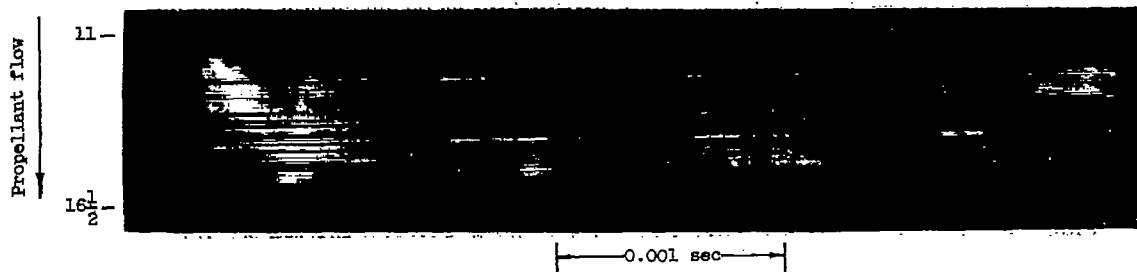


Figure 9. - Streak photographs showing oscillations between stations 0 and  $5\frac{1}{2}$  of screaming combustion in a 1000-pound-thrust rocket engine with WFNA and JP-3 for run 3.

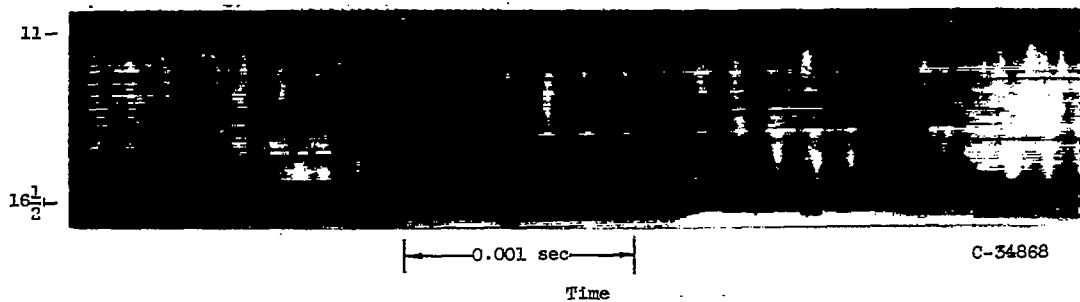
Station, in. from injector



(a) Smooth combustion prior to scream. Flow, 425 feet per second.



(b) Longitudinal oscillation (940 cps) without lateral oscillation.

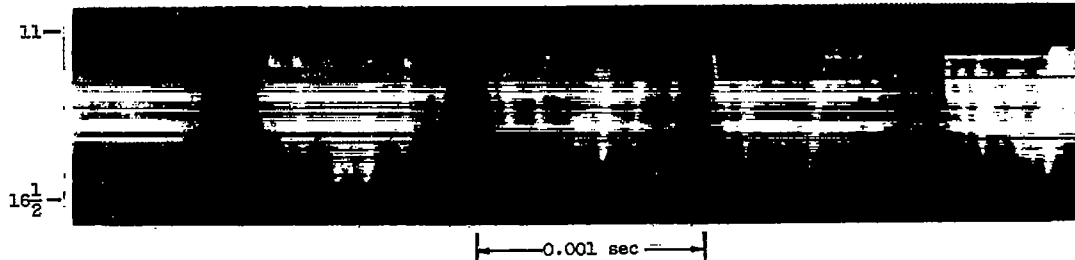


(c) Strong lateral oscillation (6000 cps) with faint longitudinal oscillation (980 cps).

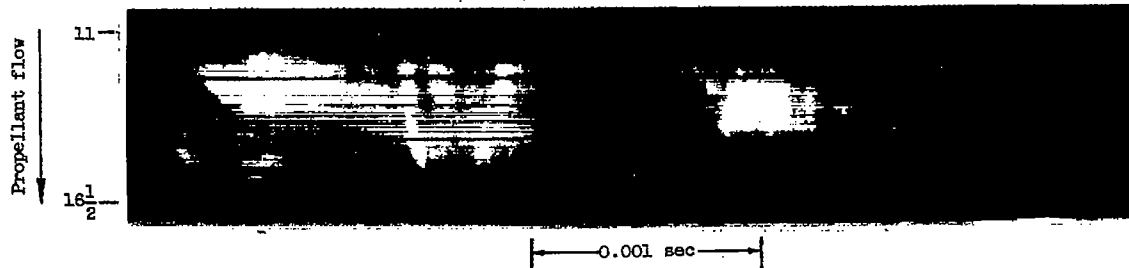
Figure 10. - Streak photographs showing oscillations between stations 11 and  $16\frac{1}{2}$  of screaming combustion in a 1000-pound-thrust rocket engine with WFNA and JP-3 for run 4.



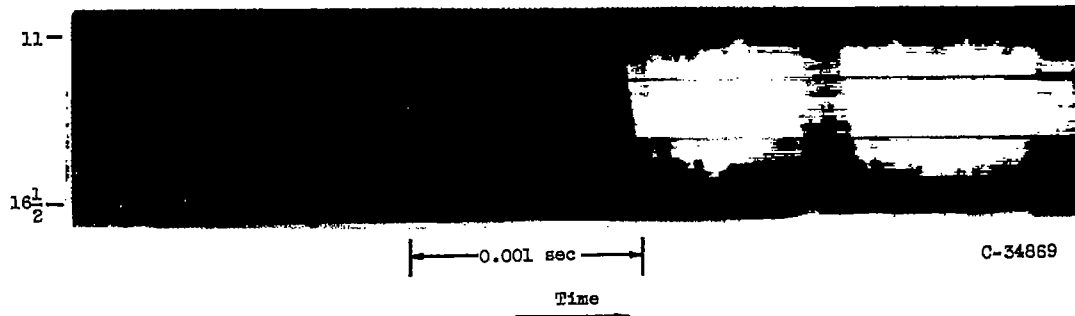
Station, in. from injector



(d) Strong longitudinal oscillation (1000 cps) distorts lateral shocks into bent (tilted) lines.



(e) Longitudinal shock lines concurrent with lateral oscillation. First longitudinal cycle shows flow reversal.



C-34869

(f) Shock waves appear to influence intensity of combustion if luminosity is criterion of combustion intensity.

Figure 10. - Concluded. Streak photographs showing oscillations between stations 11 and  $16\frac{1}{2}$  of screaming combustion in a 1000-pound-thrust rocket engine with WFNA and JP-3 for run 4.

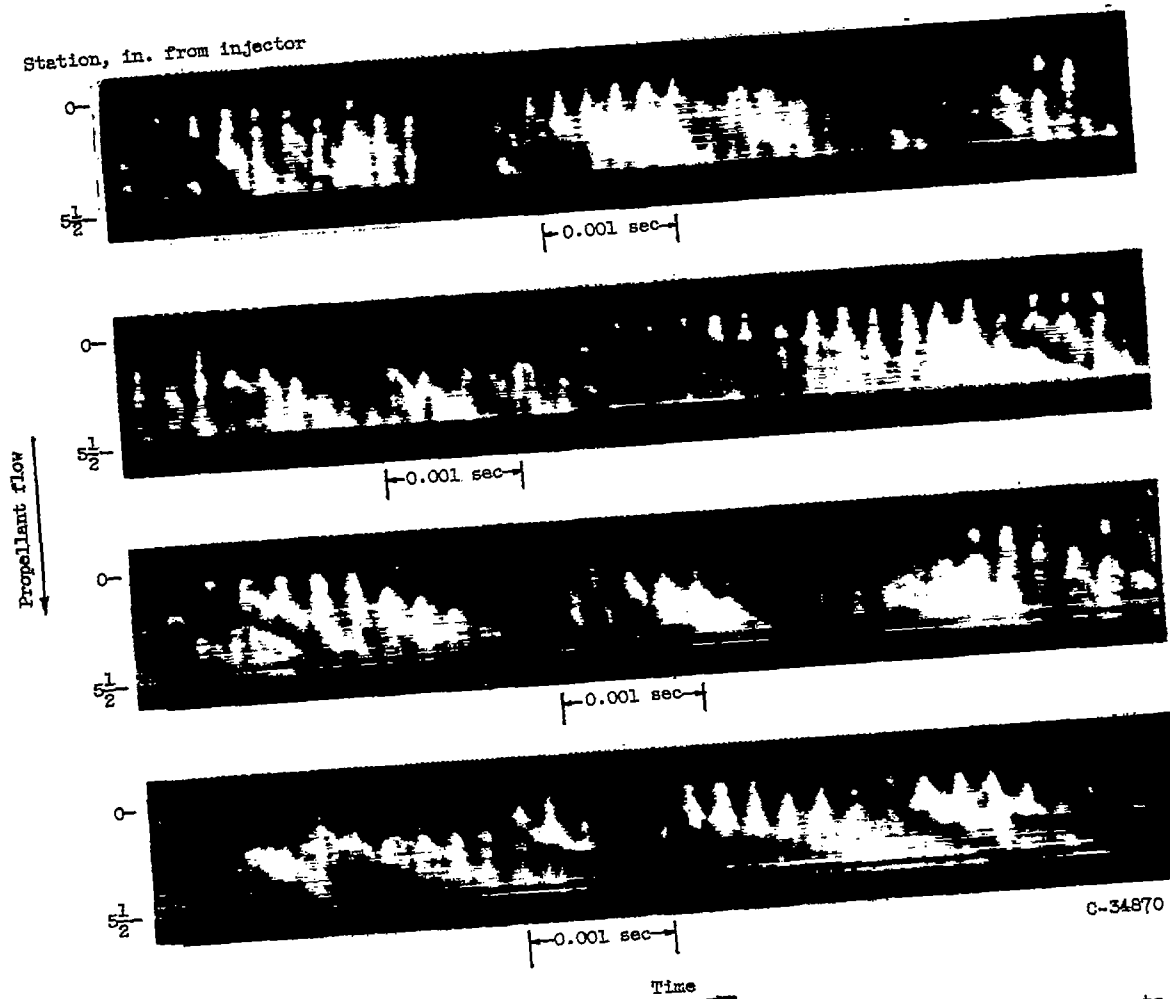
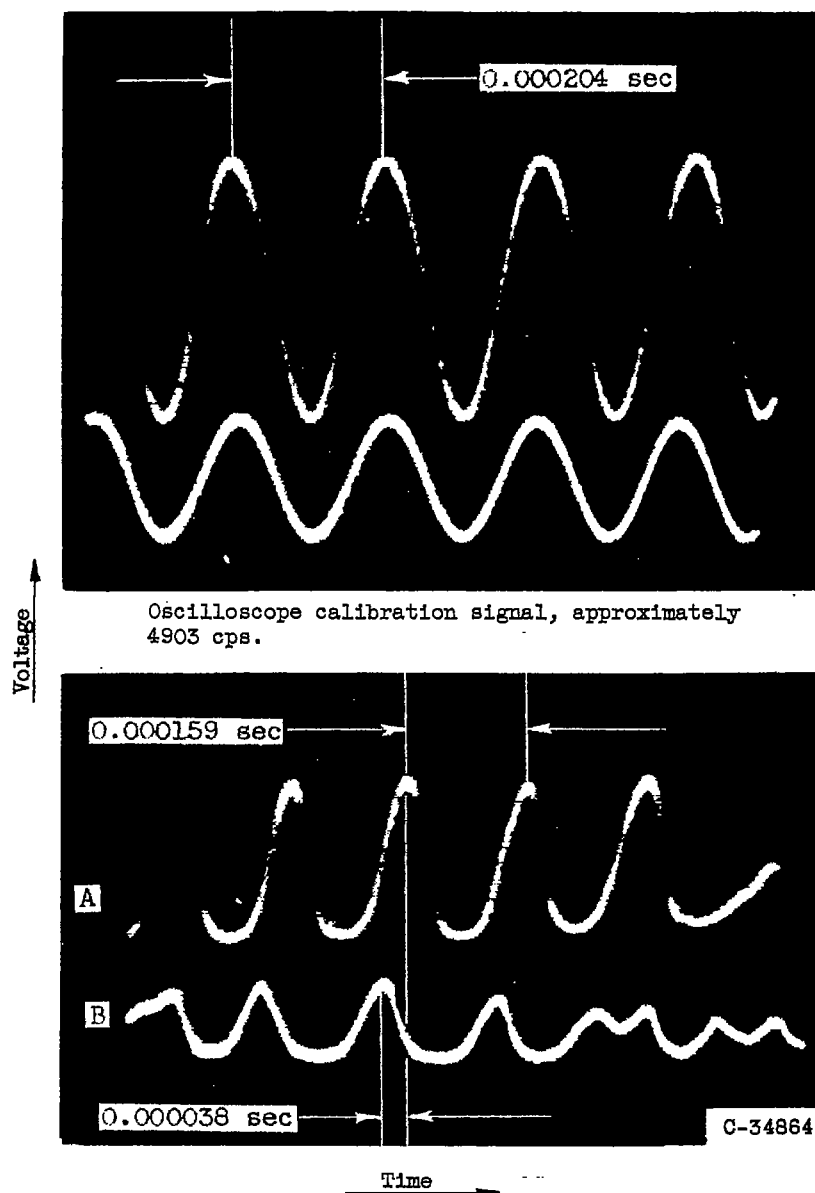


Figure 11. - Streak photographs showing lateral oscillations with longitudinal components for run 2. Lateral oscillation frequency, 4200 cps.

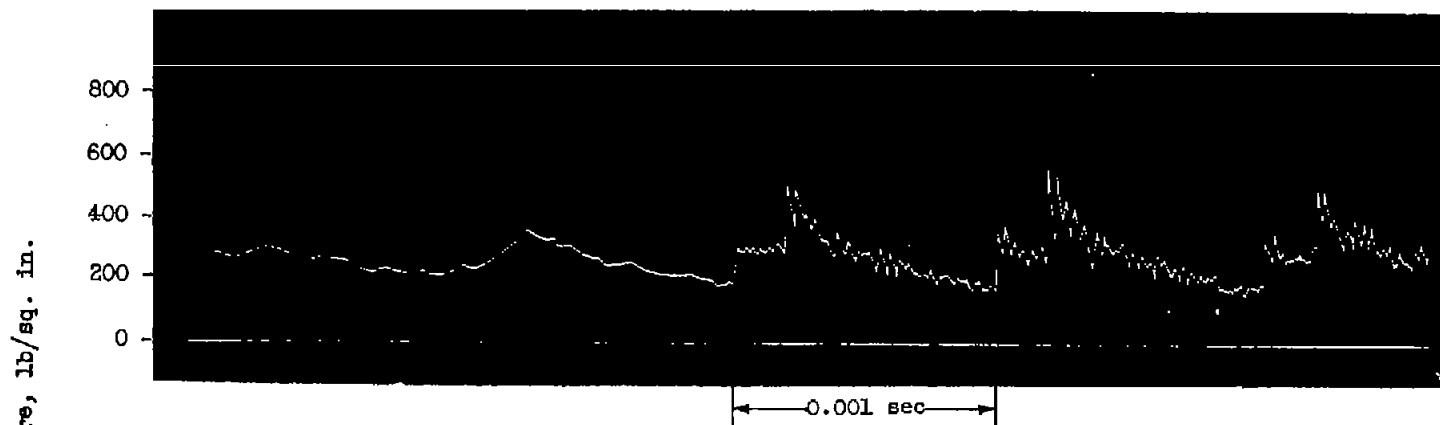
CONFIDENTIAL



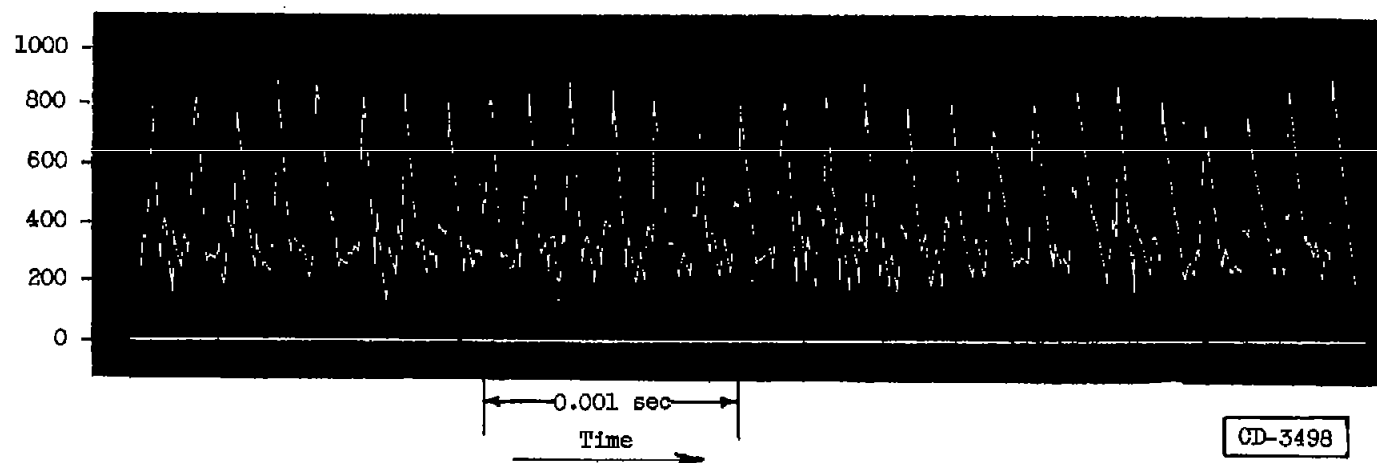
A and B placed  $90^\circ$  apart for run 2.

Frequency of cycling, 6300 cps; average displacement phasing between A and B,  $105^\circ$ .

Figure 12. - Photographs showing ion-gap voltage changes during screaming combustion of 1000-pound-thrust rocket engine with WFNA and JP-3.



(a) Development of shock-fronted longitudinal waves.



(b) High-frequency lateral oscillation.

Figure 13. - Pressure traces with flush-mounted pickup. Superimposed oscillograph traces reproduced separately for clarity.

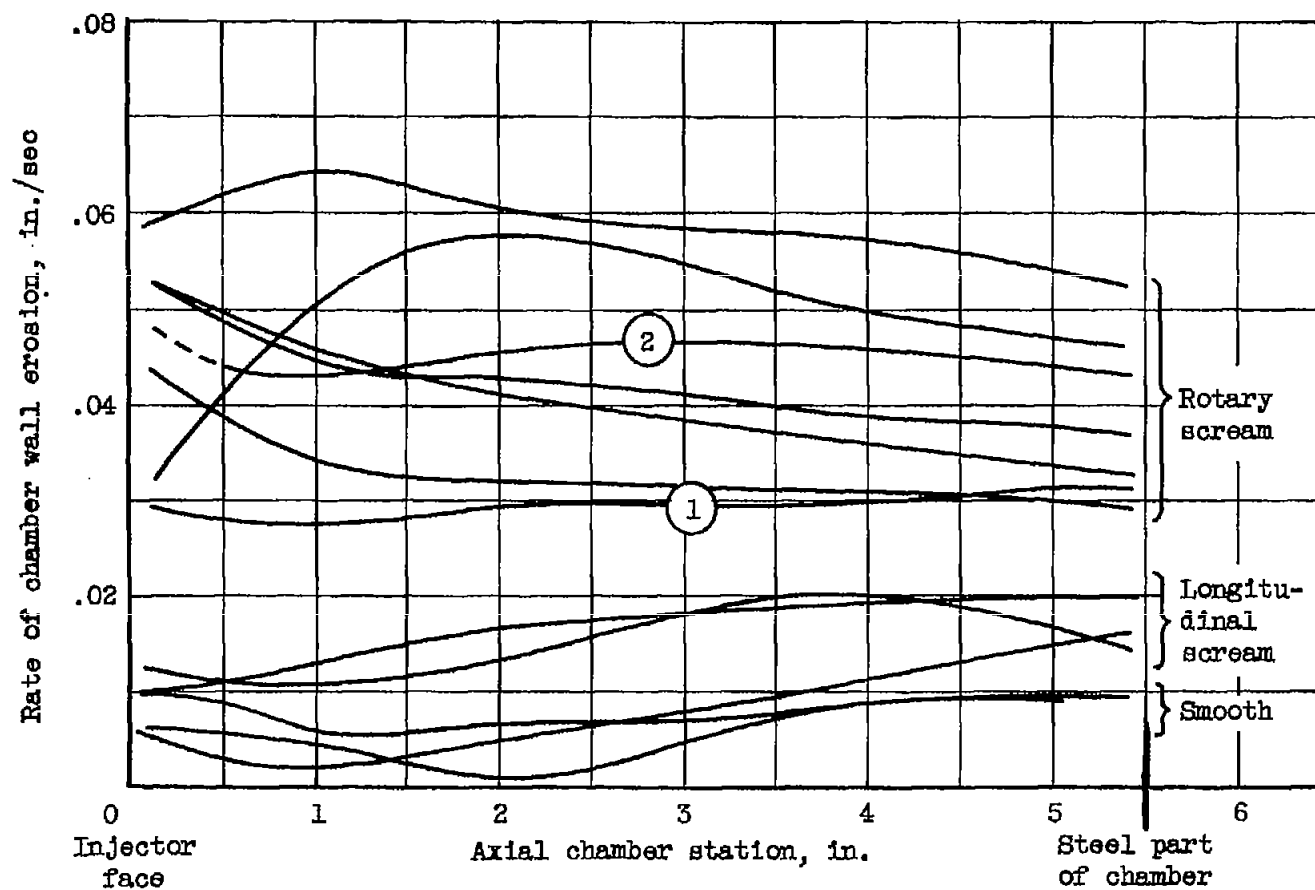
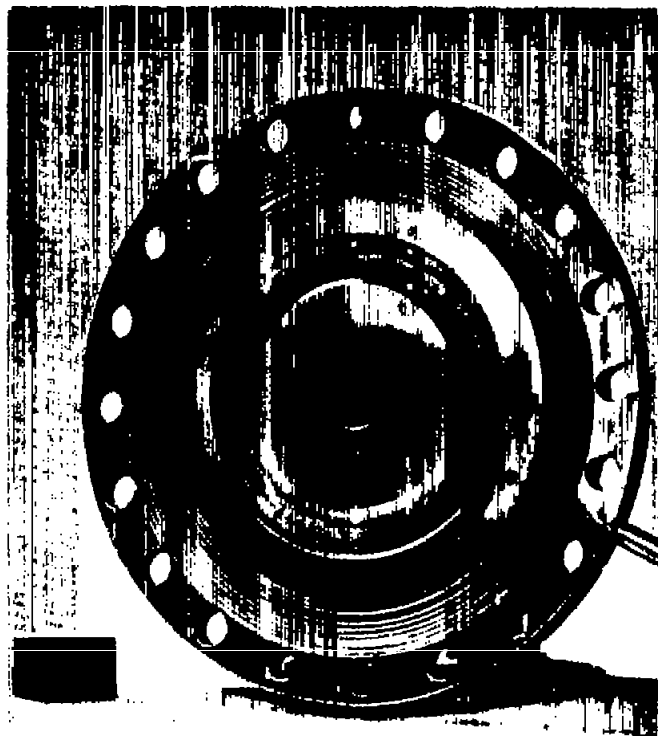
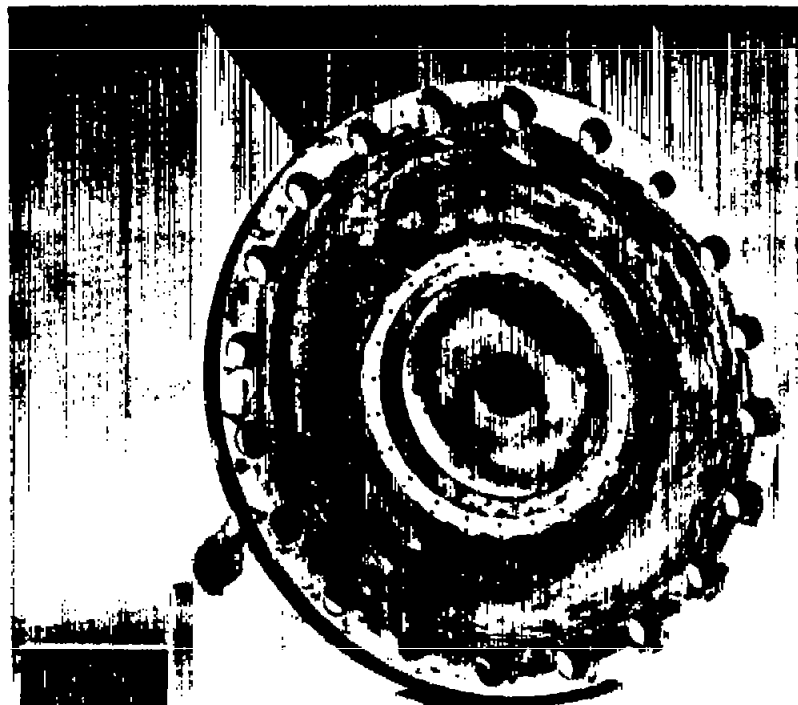


Figure 14. - Erosion rates of plastic chamber wall of 1000-pound-thrust rocket engine with WFNA and JP-3. Numbers refer to runs shown on other figures.



C-34082

(a) Before running.



C-33483

(b) After running.

Figure 15. - Injector of run 94 showing surface erosion resulting from screaming due to rotary oscillation.